Cryogenic Treatment Effect on Strength Properties of Bearing Steel for Cold Rolling Rolls

Seiji Ito[1, 2], Utata Miyoshi[2], Shohei Ueki[3], Toshiyuki Kondo[3], Shigeru Hamada[3]

[1]Research & Development, Nippon Steel Corporation
20-1 Shintomi Futtsu Chiba, Japan, 293-8511
Phone: +81-439-80-2111
Email: ito.m3d.seiji@jp.nipponsteel.com

[2]Graduate School of Engineering, Kyushu University
744 Motooka Nishi-ku Fukuoka, Japan, 819-0395

[3]Faculty of Engineering, Kyushu University,
744 Motooka Nishi-ku Fukuoka, Japan, 819-0395

Keywords: Roll, Cold strip rolling, Cryogenic treatment, Static strength, Thermal shock resistance

INTRODUCTION

Rolling elements, commonly known as spalling elements, may undergo damage during use. Spalling damage can be divided into three processes, viz. crack initiation, extension, and delamination, which occur via the following mechanisms: crack extension, caused by the cyclic loading of an initiating crack, essentially represents fatigue crack extension; spalling occurs when the fatigue crack length reaches the threshold for static failure under a load. Typically, cracks in high-strength steel originate from inclusions. In a study conducted by one of the authors on the fracture of notched high-speed steel used for hot-rolling, considering the interaction between the stress concentration due to the notch and inclusions was necessary[1, 2)]. However, the feasibility of applying this concept to bearing steels, which are sometimes utilized for cold-rolling rolls because they contain inclusions smaller than those in high-speed steels, remains unexplored. Various methods that reduce the number of inclusions and modify the microstructure have been proposed to address the spalling damage. However, a complete solution has not yet been reported.

In this study, we investigated the effect of cryogenic treatment on the strength properties of bearing steel; this treatment is expected to improve the wear resistance and mechanical properties of bearing steel. Cryogenic treatment[3)] generally involves cooling the material to a temperature ≤ −80 °C immediately after quenching. This process transforms any unstable retained austenite (γ) phase into martensite, thereby reducing dimensional changes and nonuniform hardness over time. Cryogenic treatment is expected to enhance strength properties because it minimizes the content of austenite retained in the material.

In the initial phase of this study, we focused on evaluating the mechanisms of crack initiation in bearing steels, not subjected to cryogenic treatment, via specific tests, including tensile tests of both smooth and notched materials and drop-weight thermal shock tests[4)]. Tensile tests were performed to confirm the static strength of the target-bearing steel, whereas in the drop-weight thermal shock test, the impact of a foreign object was simulated. During this test, the potential energy of a falling weight was converted into the kinetic energy of a carbon steel object, which then slid against the test object at a high speed, replicating the conditions of a foreign object impact. This test revealed the thermal crack initiation behavior driven by rapid temperature changes during friction.

TESTING METHODS

To evaluate the tensile strength properties, including the underlying mechanisms, bearing steel specimens, without cryogenic treatment, were subjected to smooth-material tensile tests. Additionally, notched-material tensile tests were conducted to assess the impact of stress concentration on the tensile strength properties. Thermal shock tests were also performed to examine the crack initiation behavior.

Test Material

Table 1 lists the compositions of the test material, i.e., a bearing steel (specified as SUJ2 in the Japanese Industrial Standards).

Figure 1 shows the heat-treatment conditions of the test material. Spheroidizing annealing was performed at 795 °C for 90 min, followed by quenching at 880 °C for 30 min. The specimens were tempered at 150 °C for 120 min without cryogenic treatment. The amount of retained austenite in the specimens was measured by X-ray diffraction.

Table 1. Composition of bearing steel used as the test material (mass%).

C	Si	Mn	Cr	Mo	Fe
0.96	0.17	0.29	1.33	0.04	Bal.

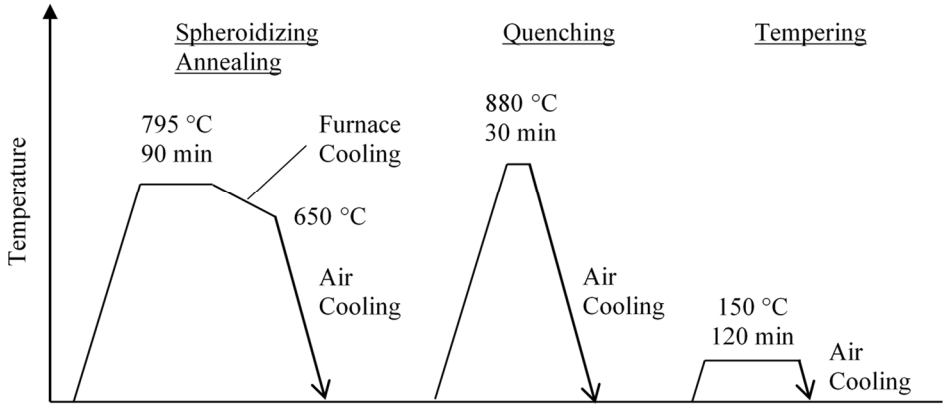

Figure 1. Heat-treatment conditions of the test material.

Tensile Test

Figure 2 illustrates the geometry of the smooth specimens used in the tensile test, and Figure 3 shows the geometry of the notched specimens. The radii of curvature (ρ) of the notched specimens were 0.4, 0.7, 1.0, and 3.0 mm. The tests were conducted using an electrohydraulic servo fatigue testing machine (Model EHF-EV051K1-010-1A) manufactured by Shimadzu Corporation. After the test, the fracture surfaces were examined using scanning electron microscopy (SEM) to determine the fracture mechanisms.

Drop-Weight Thermal Shock Test

Figure 4 shows a schematic of the drop-weight thermal shock test. The specimens were subjected to high-speed friction due to a high surface pressure, between a mild steel wire rod simulating the rolled material and a test specimen, using a thermal shock tester. This tester utilized the energy from a falling weight to apply thermal shock to the specimens, mimicking the impact of foreign object bites. The specimens subjected to thermal shock tests were sectioned at the center of the friction zone, mirror-polished, etched, and examined using SEM. The initiated crack length and heat-affected layer thickness were measured using SEM to establish their correlation with crack initiation.

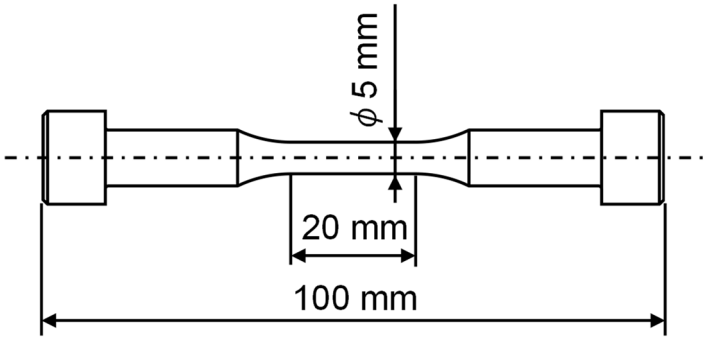

Figure 2. Shapes and dimensions of the smooth specimen.

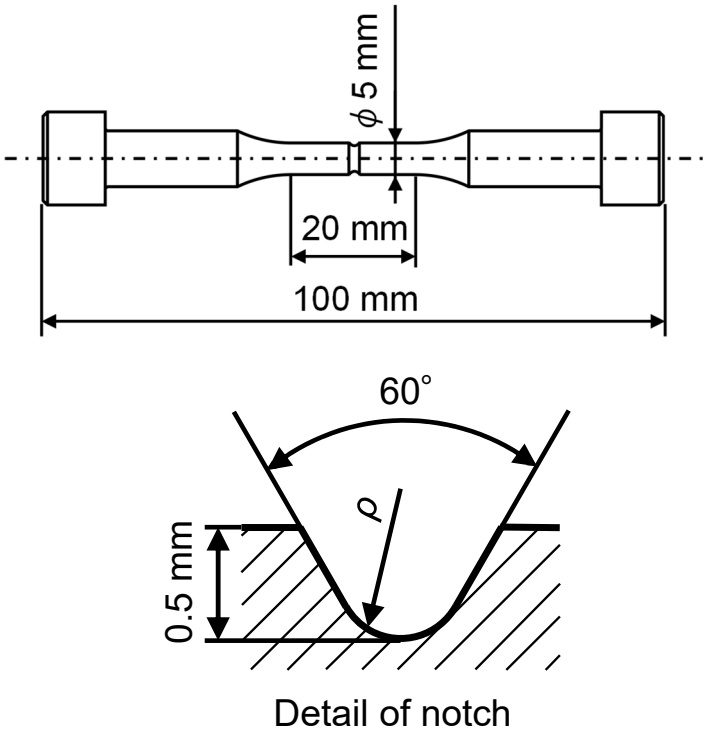

Figure 3. Shapes and dimensions of the notched specimen.

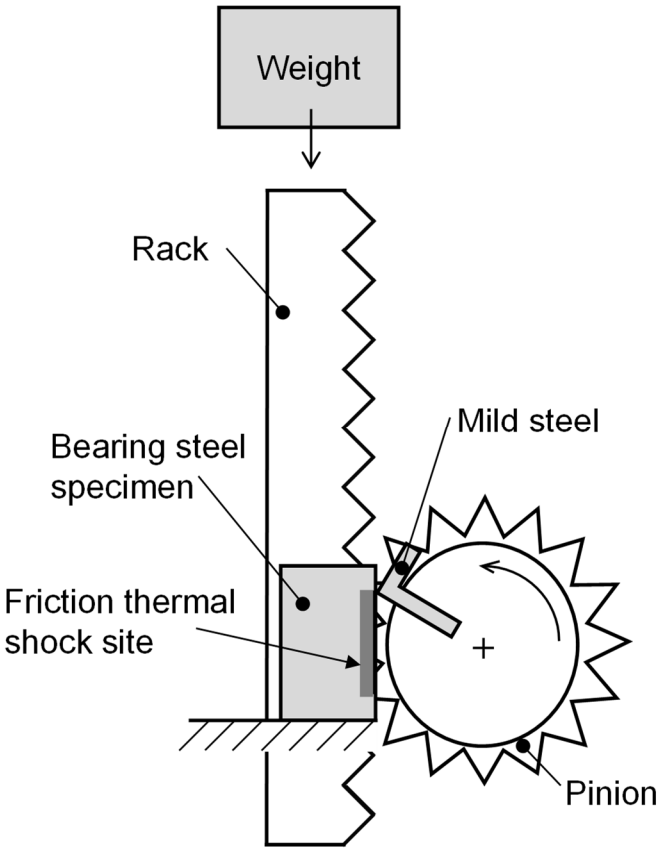

Figure 4. Schematic of the drop-weight thermal shock test.

RESULTS AND DISCUSSION

Smooth Tensile Test

Figure 5 shows the SEM images of the fracture surface. Although high-strength steels generally exhibit fracture behavior driven by inclusions, the fracture surfaces observed in this study confirm that the inclusions in the specimen are sufficiently small and do not serve as initiation points for fractures. The fracture initiation points of the bearing steel specimens used in this study are internal intergranular fractures. The fracture process is assumed to proceed as follows: Under increasing tensile loading, intergranular cracks are initiated, and they stably extend along the grain boundaries, eventually leading to an unstable fracture.

Unstable fracture in bearing steel fracture can be evaluated by examining the critical stress intensity factor (K_C). Table 2 presents the tensile strength, critical stress intensity factor, Vickers hardness, and residual austenite content of the bearing steel specimens not subjected to cryogenic treatment. The critical stress intensity factor value is calculated by treating the intergranular fracture zone, specifically the stable crack extension zone just before the unstable fracture, as a pre-existing crack and using Murakami's method, which estimates the stress intensity factor using $\sqrt{area}$ under tensile loading[5].

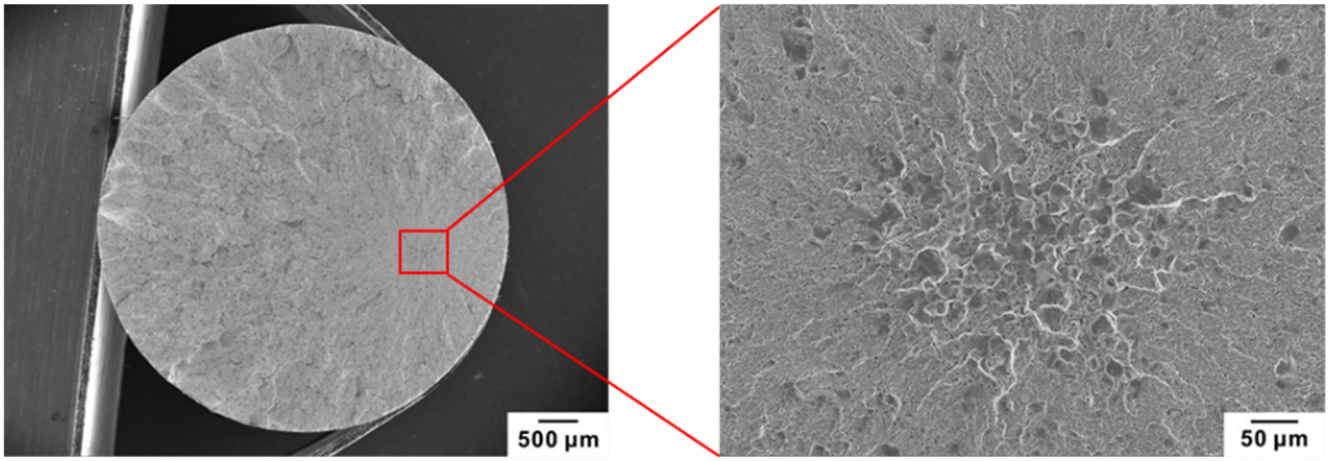

Figure 5. Fracture surface of the bearing steel specimen.

Table 2. Mechanical properties and amount of austenite retained in the bearing steel specimen not subjected to cryogenic treatment.

Tensile strength σ_{uts} [MPa]	Critical stress intensity factor value K_C [MPa$\sqrt{m}$]	Vickers hardness HV [kgf/mm^2]	Retained austenite content [vol. %]
1690	24.0	796	19

Notched Tensile Test

Figure 6 shows the tensile-test results of the notched specimens, indicating the tensile strength as a function of the reciprocal of the notch radius of curvature, $1/\rho$. The smooth specimen is considered to have a ρ value of infinity, and its results are plotted at the position where $1/\rho$ equal to zero. Evidently, the smooth specimen shows the highest tensile strength, and the strength decreases monotonically with increasing $1/\rho$, confirming the absence of notch strengthening in the bearing steel. Consequently, given that bearing steels fail before undergoing plastic deformation, their strength properties must be evaluated based on their crack behavior rather than notch strengthening.

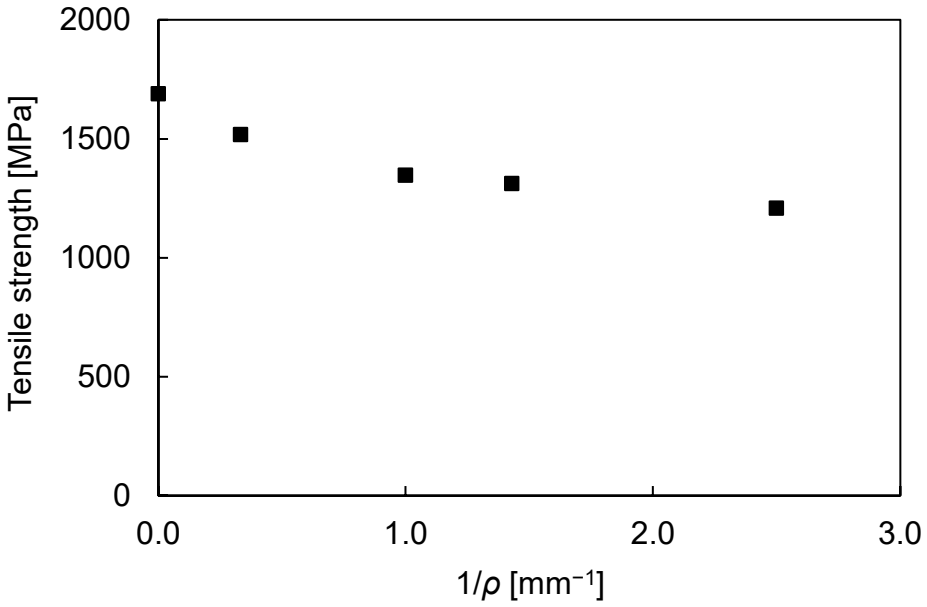

Figure 6. Relationship between tensile strength and $1/\rho$; ρ represents the notch's radius of curvature.

Thermal Shock Test

Figure 7 presents cross-sectional SEM images of the thermal shock zone of the specimen. Thermal cracks are not initiated in the cryogenic-treatment-free bearing steel specimen. This result suggests that a high amount of retained austenite enhances the resistance to thermal cracking. The detailed analysis results of the thermal shock test are presented in this paper.

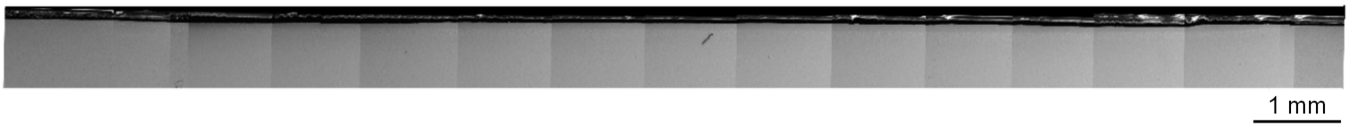

Figure 7. Cross-sectional SEM images of the thermal shock area of the cryogenic-treatment-free specimen.

CONCLUSIONS

1. The initial fracture point of the bearing steel, used in this study, under static tensile loading was an intergranular fracture that occurred through an unstable fracture mechanism following the stable fracture of the grain boundary.
2. No notch strengthening was observed in the bearing steel. Because bearing steels fail before the occurrence of plastic deformation, their strength properties must be analyzed in terms of crack behavior.
3. Thermal cracks were not initiated in the cryogenic-treatment-free bearing steel.

REFERENCES

1. S. Hamada, S. Kashiwagi, A. Sonoda, N. Izumi, H. Noguchi, *Evaluation of Notch Tensile Strength for High Strength Steel with Inclusions (In Case of Casting High Speed Steel)*, Trans. Jpn. Soc. Mech. Eng. Ser. A, 75, 760, 2009, p. 1764 (in Japanese).
2. A. Sonoda, S. Kashiwagi, S. Hamada, H. Noguchi, *Quantitative Evaluation of Heat Crack Initiation Condition Under Thermal Shock*, J. Solid Mech. Mater. Eng., 2, 1, 2008, p. 128.
3. N. S. Kalsi, R. Sehgal, V. S. Sharma, *Cryogenic Treatment of Tool Materials: A Review*, Mater. Manuf. Process., 25, 10, 2010, p. 1077.
4. N. Oda, P. Fleiner, T. Hattori, *Latest Developments of a New Technology HSS Work Roll for Later Stands (F4-F7) in Hot Strip Mill Finishing Trains*, Iron Steel Technol., 10, 11, 2013, p. 56.
5. Y. Murakami, *Metal Fatigue: Effects of Small Defects and Nonmetallic Inclusions, 2nd ed.*, Academic Press, 2019, p. 39.

